Electronic Supporting Information For:

Enhanced MMLCT Character in Thiol-Bridged Pt(II) Dimers Featuring Tridentate Cyclometalating Ligands

*Sarah Kromer, Liam J. Dress, Evgeny O. Danilov, Livia I. Cohen, Adrienne P. Faulkner, and Felix N. Castellano**

Department of Chemistry, North Carolina State University, Raleigh, NC 27695-8204, USA

*Correspondence: *fncastel@ncsu.edu*

Synthesis and Characterization

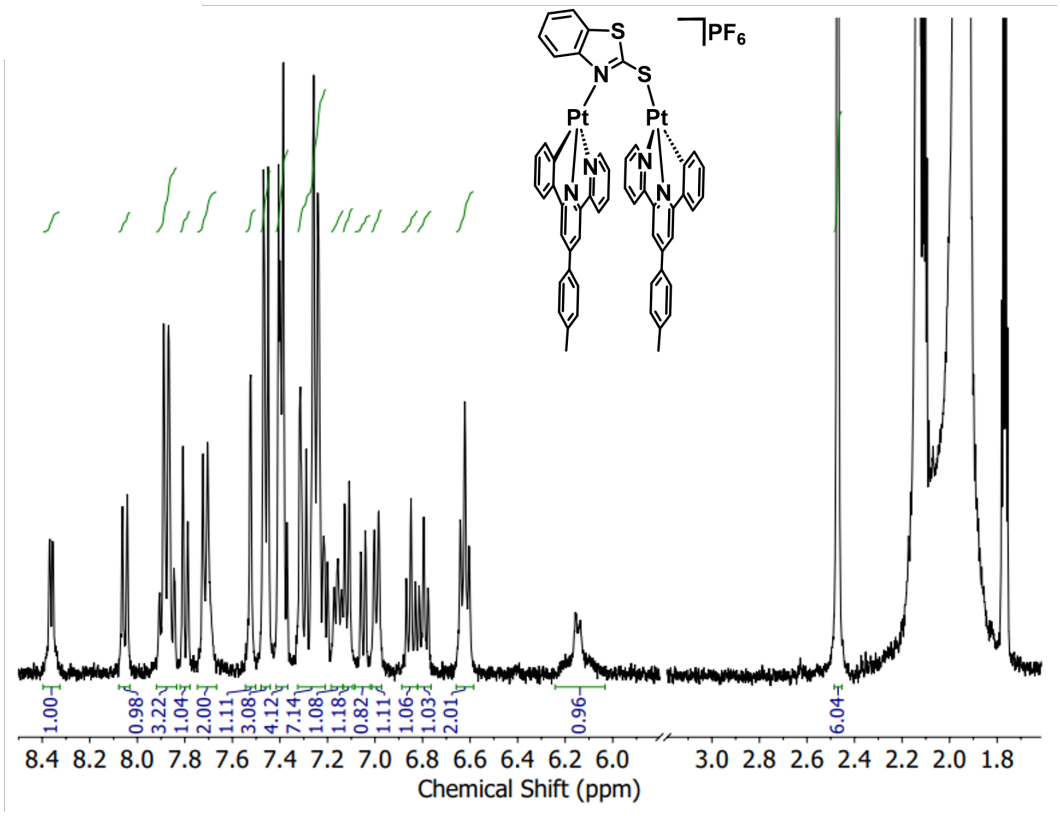

Figure S1. ^{1}H NMR spectrum (400 MHz) of **2** recorded in CD_3CN.

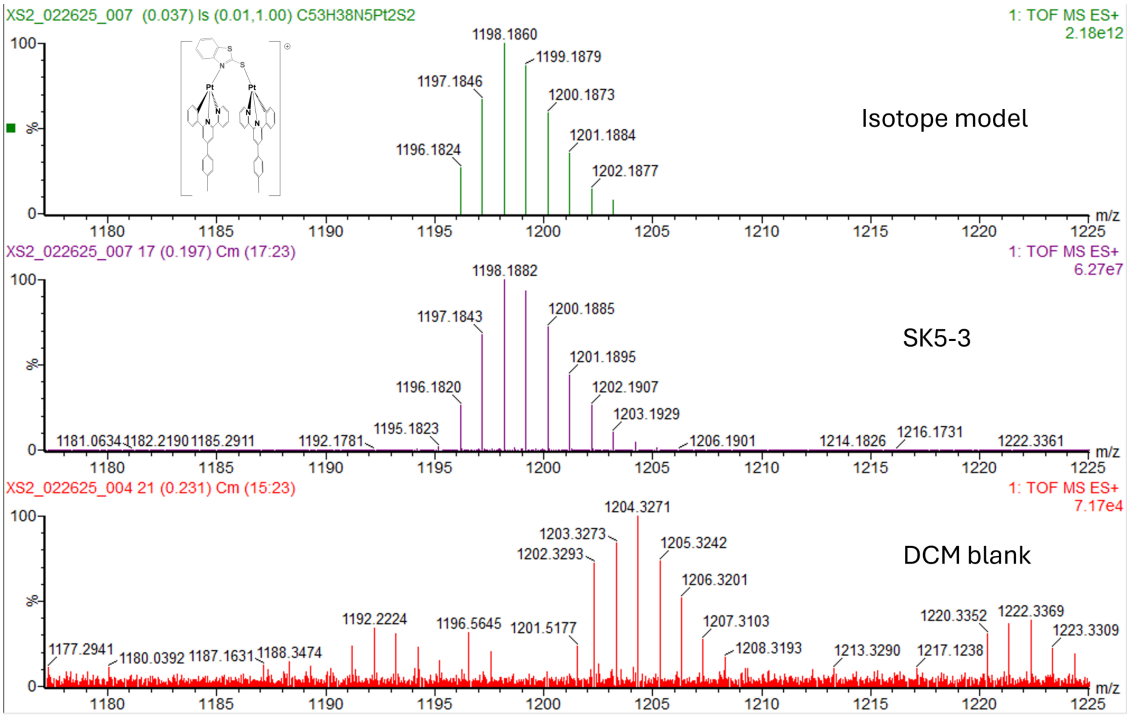

Figure S2. High resolution mass spectrum of **2**; TOF-MS-ES+ (CH_2Cl_2) *m/z*: 1,198.1882 $[M\text{-}PF_6]^+$, calcd. ($C_{53}H_{38}N_5Pt_2S_2$) 1,198.1860.

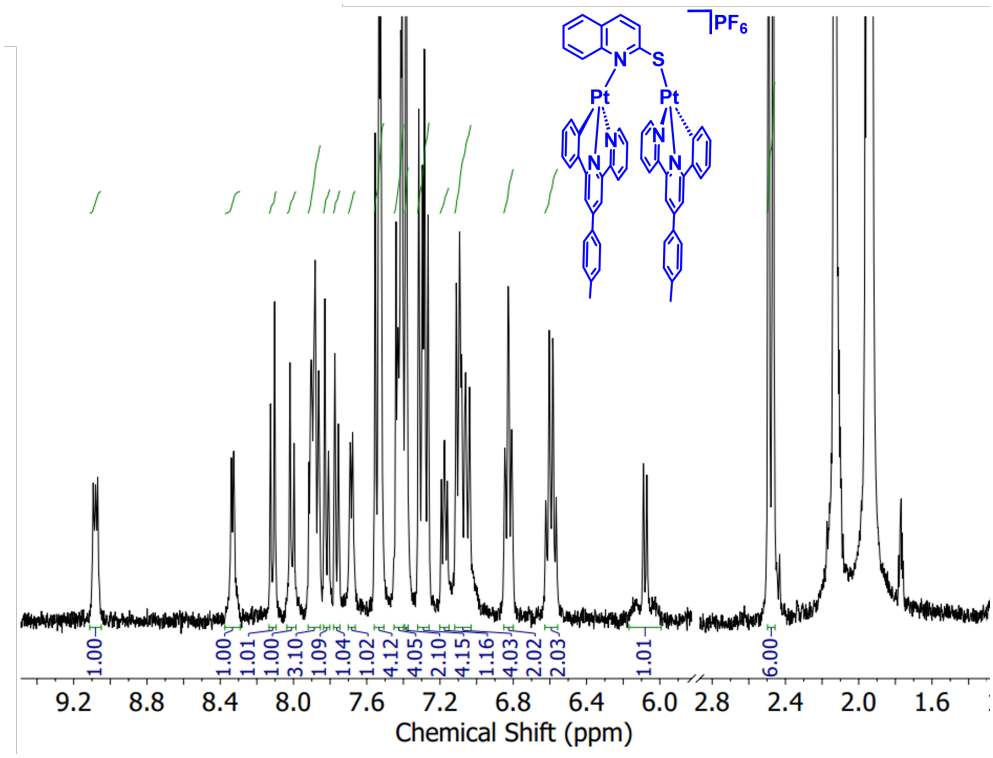

Figure S3. ^1H NMR spectrum (400 MHz) of **3** recorded in CD_3CN.

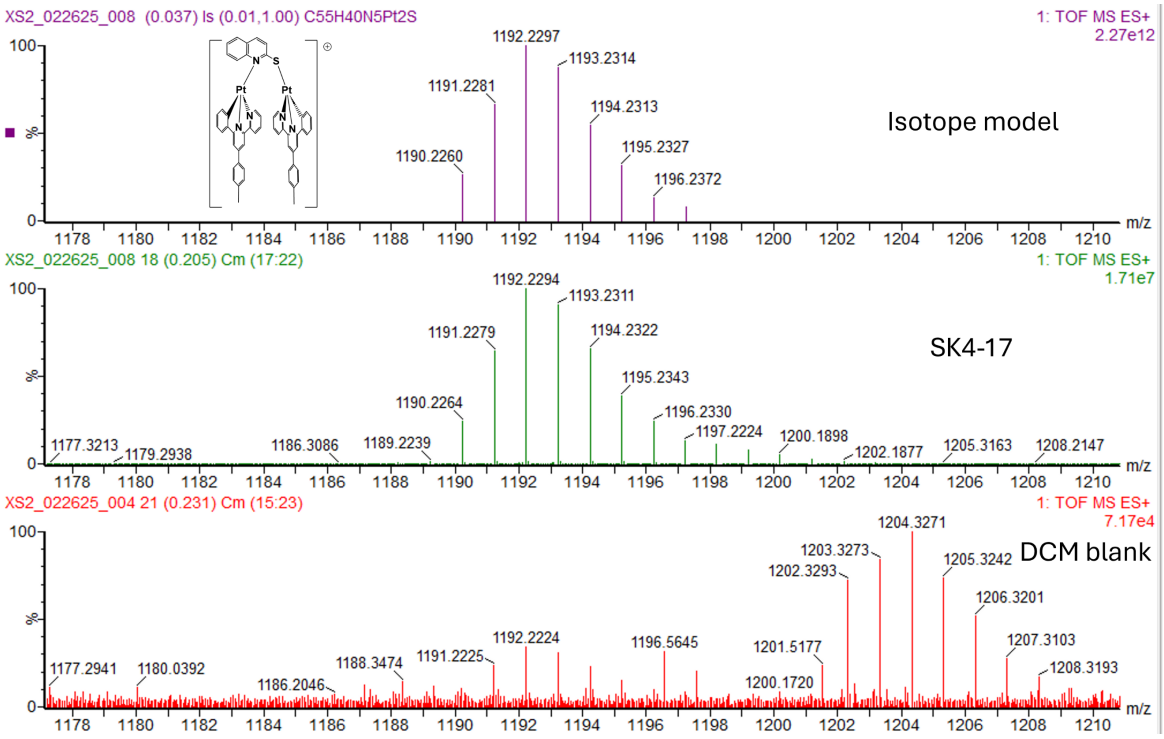

Figure S4. High resolution mass spectrum of **3**; TOF-MS-ES+ (CH_2Cl_2) *m/z*: 1,192.2294 $[M\text{-}PF_6]^+$, calcd. ($C_{55}H_{40}N_5Pt_2S$) 1,192.2297.

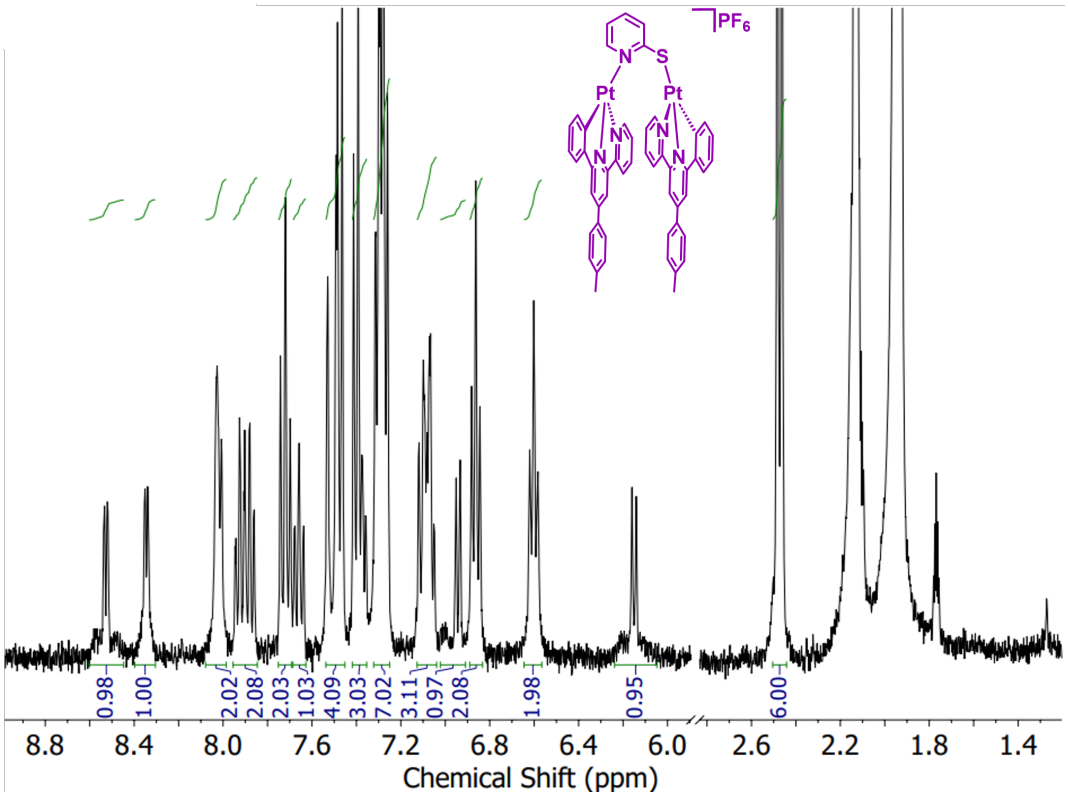

Figure S5. ^1H NMR spectrum (400 MHz) of **4** recorded in CD_3CN.

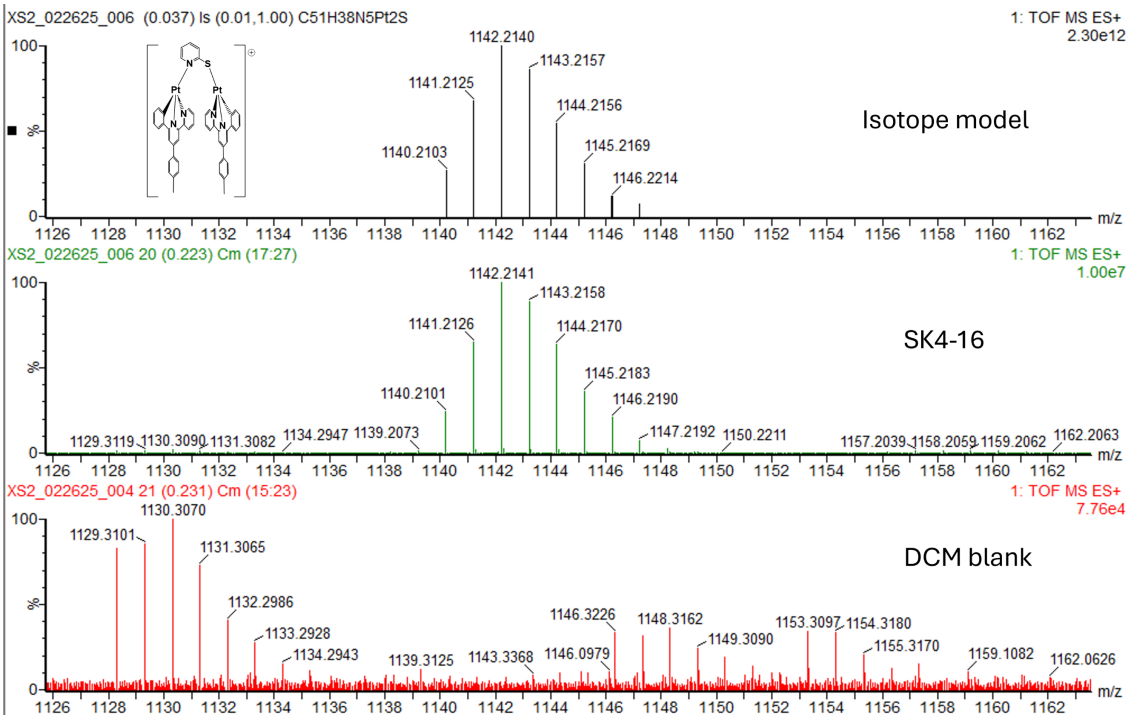

Figure S6. High resolution mass spectrum of **4**; TOF-MS-ES+ (CH_2Cl_2) *m/z*: 1,142.2141 $[M\text{-}PF_6]^+$, calcd. ($C_{51}H_{38}N_5Pt_2S$) 1,142.2140.

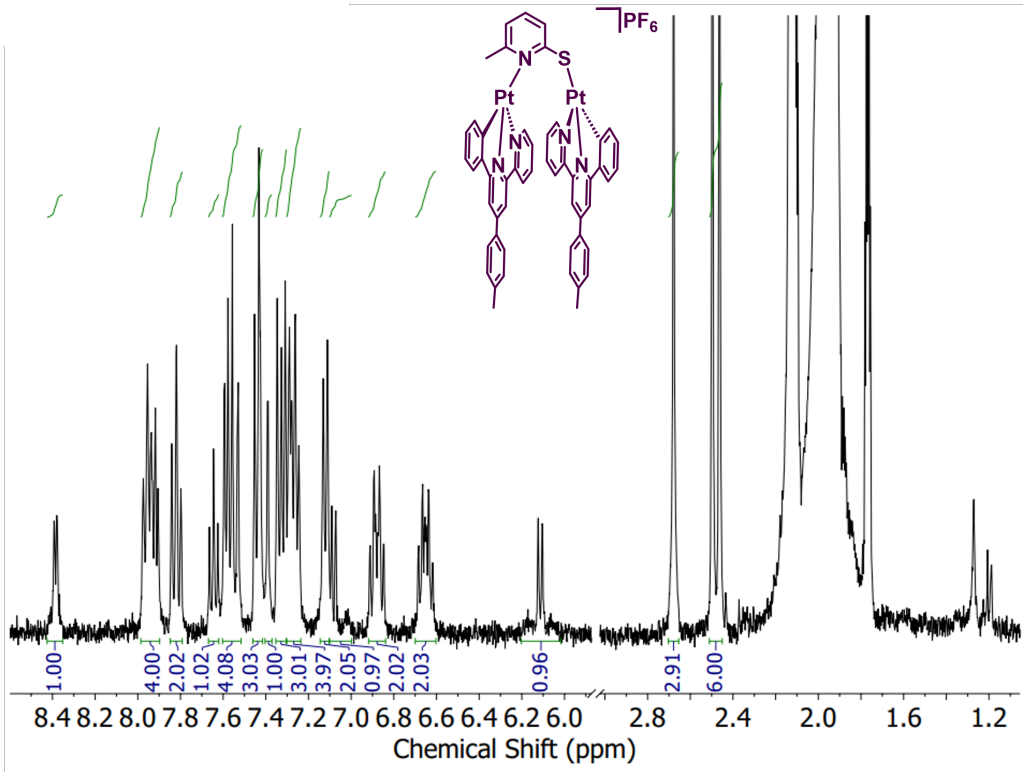

Figure S7. ^1H NMR spectrum (400 MHz) of **5** recorded in CD_3CN.

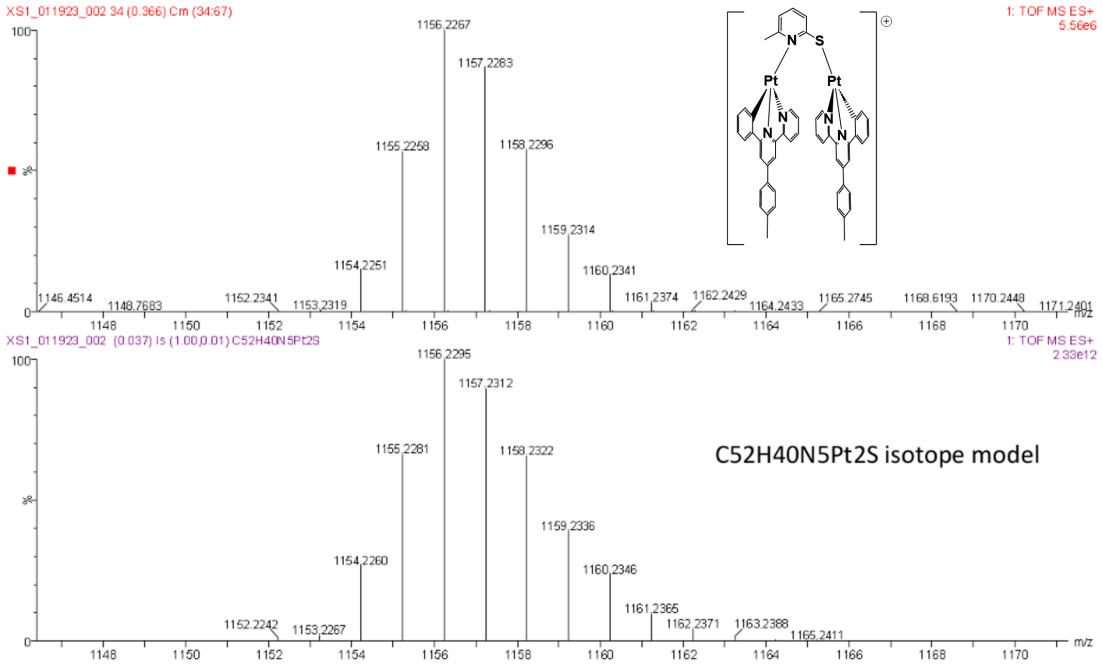

Figure S8. High resolution mass spectrum of **5**; TOF-MS-ES+ (CH_2Cl_2) *m/z*: 1,156.2267 $[M\text{-}PF_6]^+$, calcd. ($C_{52}H_{40}N_5Pt_2S$) 1,156.2295.

Photoluminescence and Excitation Spectra: Characterization of the ^{3}MMLCT Excited State:

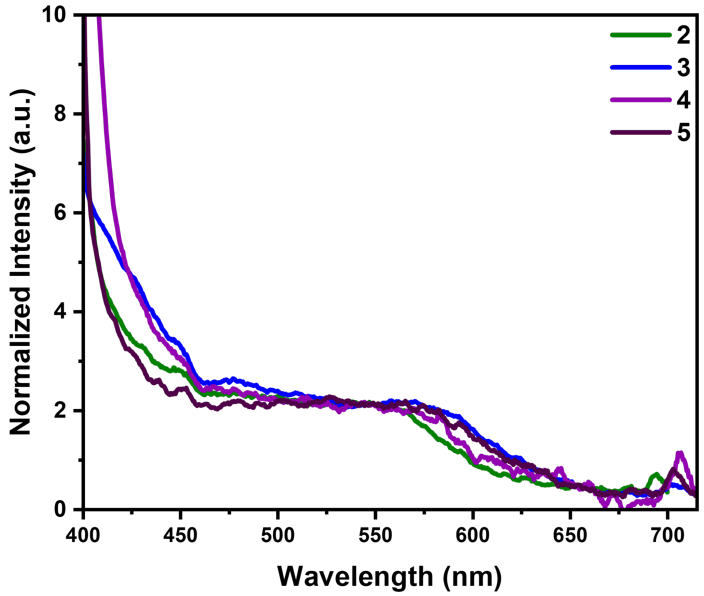

Figure S9. Combined excitation spectra of **2-5** collected by detection at the emission maximum in MeCN. The PL energies of detection are as follows: **2** (green, $\lambda_{detection}$ = 775 nm); **3** (blue, $\lambda_{detection}$ = 784 nm); **4** (purple, $\lambda_{detection}$ = 788 nm); **5** (dark purple, $\lambda_{detection}$ = 785 nm).

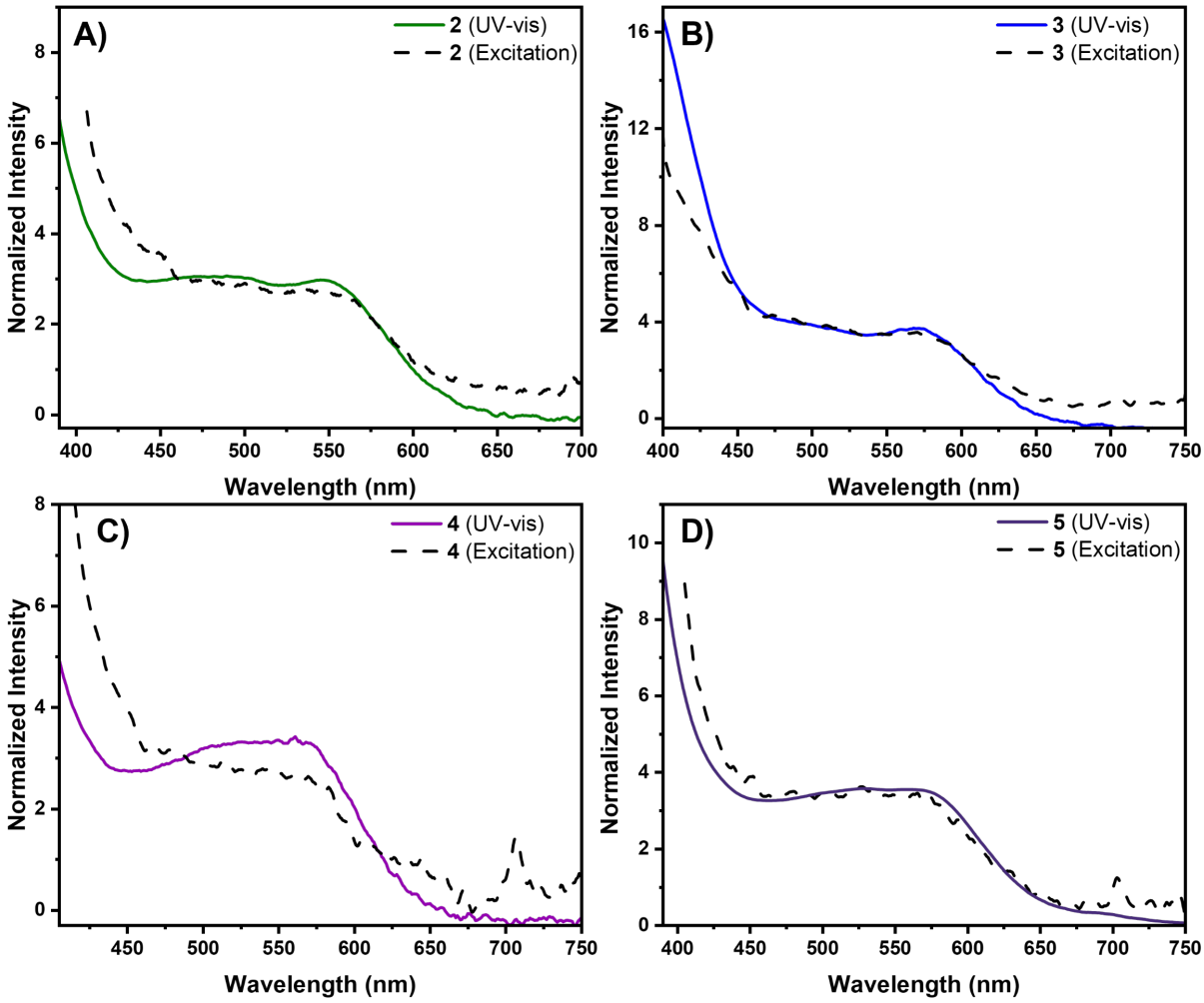

Figure S10. Comparison of the MMLCT absorbance bands collected by UV-vis with excitation scans measured by detection at the MMLCT emission maximum of **2-5** in MeCN. **A) 2** ($\lambda_{detection}$ = 775 nm); **B) 3** ($\lambda_{detection}$ = 784 nm); **C) 4** ($\lambda_{detection}$ = 788 nm); and **D) 5** ($\lambda_{detection}$ = 785 nm).

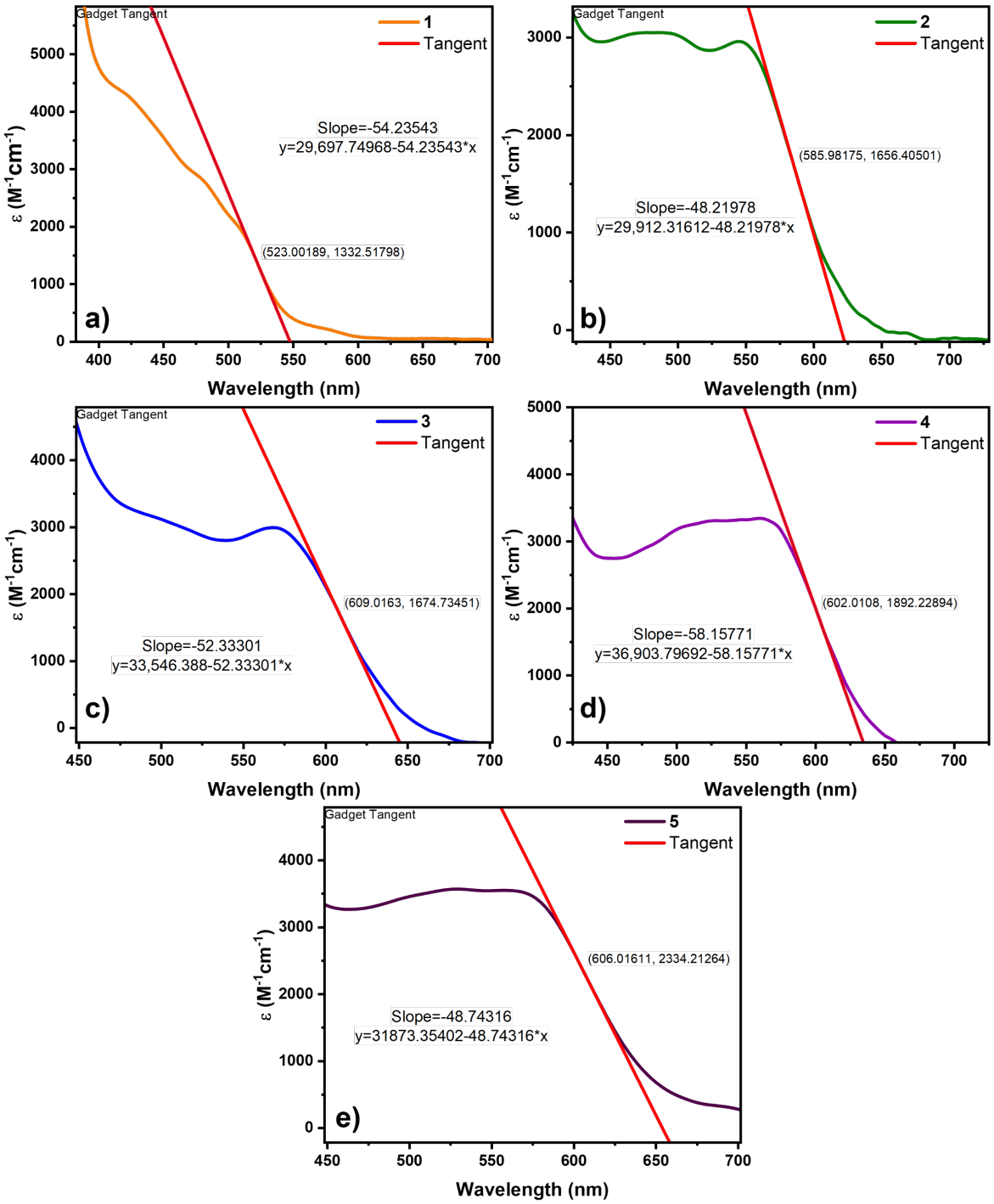

Figure S11. Tangent analysis of the red edge of the MMLCT absorption feature measured in MeCN to estimate the ^{1}MMLCT state energy. The estimated ^{1}MMLCT excited state energies of **1-5** based on the x-intercept of the tangent line are: **a) 1**, 547.6 nm, 18,262.5 cm^{-1}; **b) 2**, 620.3 nm, 16,120.4 cm^{-1}; **c) 3**, 641.0 nm, 15,600.2 cm^{-1}; **d) 4**, 634.5 nm, 15,759.3 cm^{-1}; and **e) 5**, 653.9 nm, 15,292.9 cm^{-1}.

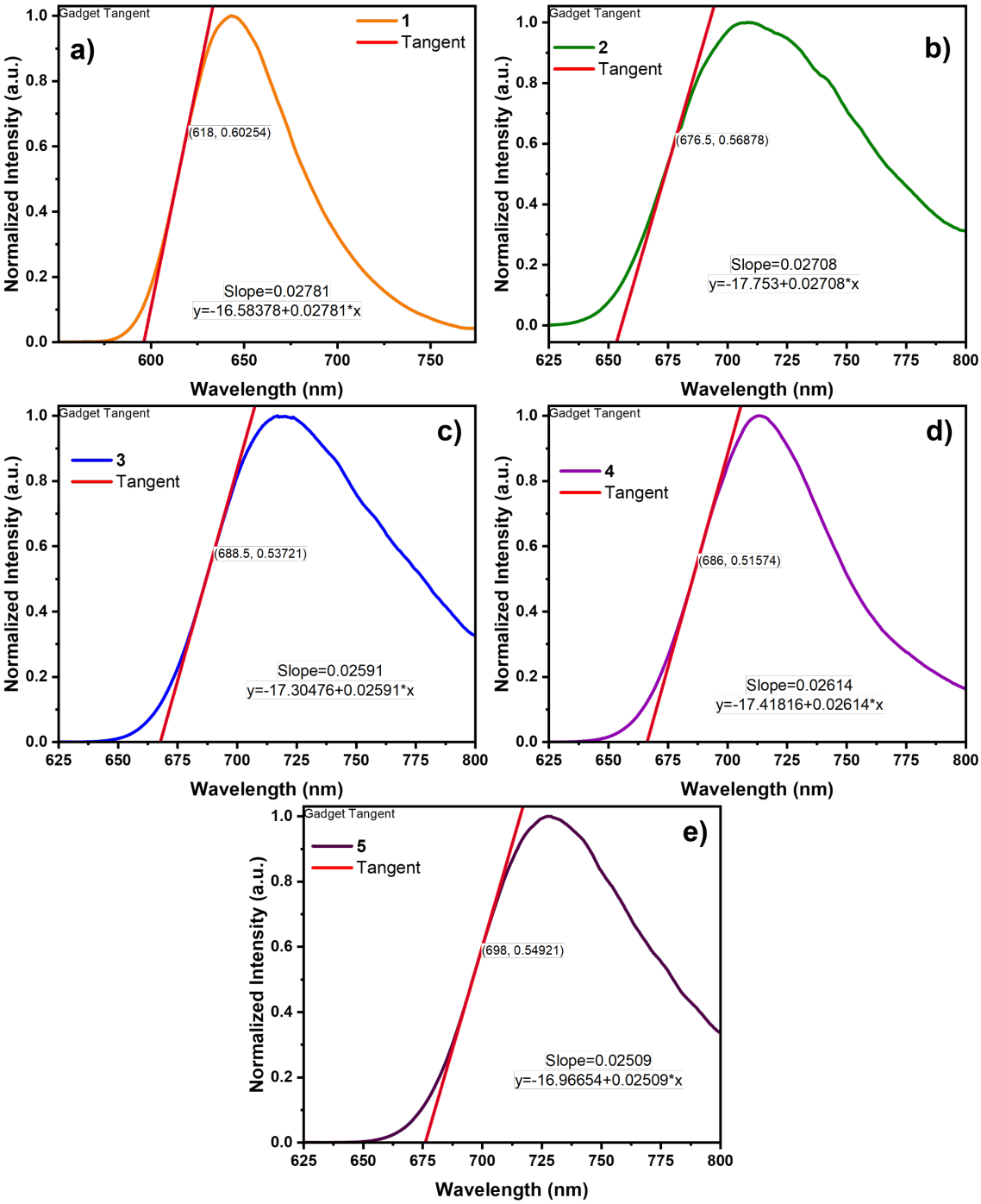

Figure S12. Tangent analysis of the ^{3}MMLCT PL feature measured in butyronitrile at 77 K following excitation at 500 nm (**1**) and 560 nm **(2-5**). The estimated ^{3}MMLCT excited state energies of **1-5** based on the x-intercept of the tangent line are: **a) 1**, 596.3 nm, 16,769.4 cm^{-1}; **b) 2**, 655.6 nm, 15,253.8 cm^{-1}; **c) 3**, 667.9 nm, 14,972.8 cm^{-1}; **d) 4**, 666.3 nm, 15,007.3 cm^{-1}; and **e) 5**, 676.2 nm, 14,787.9 cm^{-1}.

Time-Resolved PL – ^{3}MMLCT lifetimes:

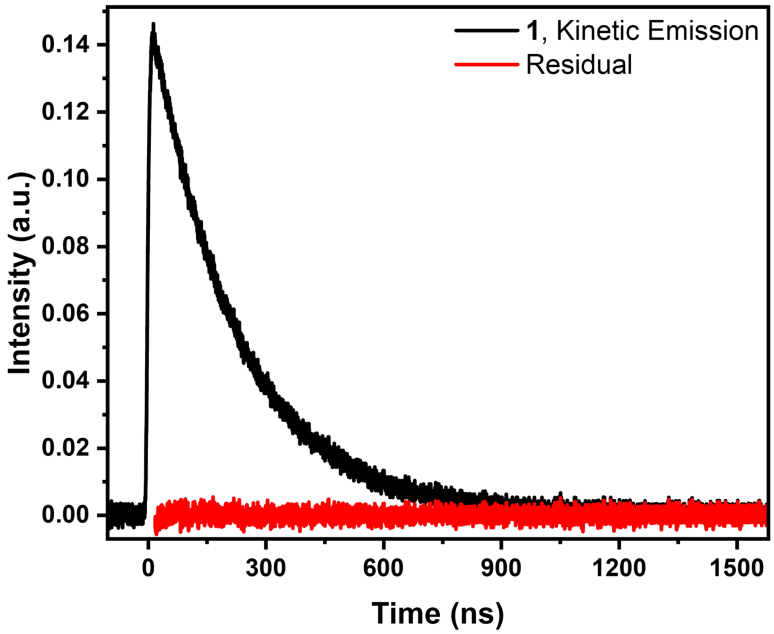

Figure S13. Kinetic emission decay of **1** collected in MeCN by excitation at 500 nm (1.2 mJ/pulse) by an Edinburgh LP900. Single-wavelength kinetics analysis determined lifetime of τ_{PL} = 216.2 ± 0.3 ns

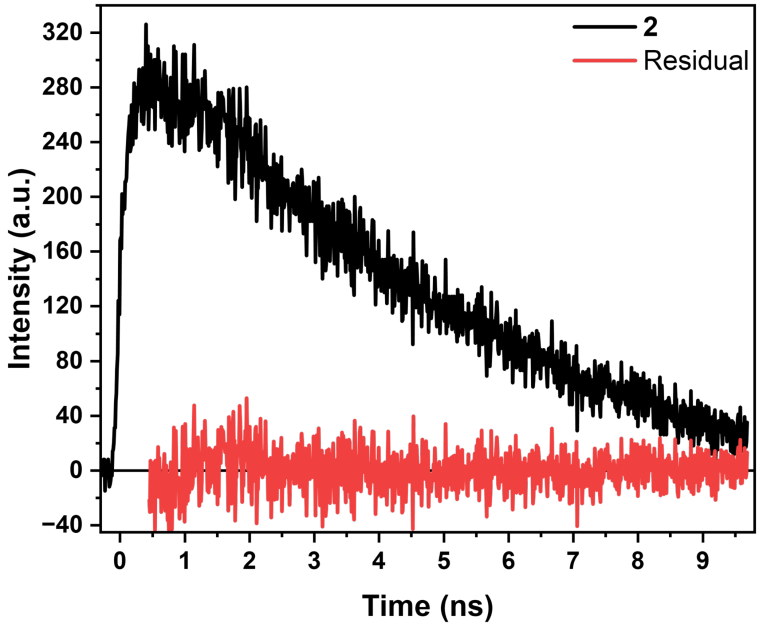

Figure S14. Kinetic emission decay of **2** collected in MeCN by excitation at 570 nm (0.2 nJ/pulse) on a LifeSpec II TCSPC. Single-wavelength kinetics analysis determined lifetime of τ_{PL} = 7.5 ± 0.3 ns

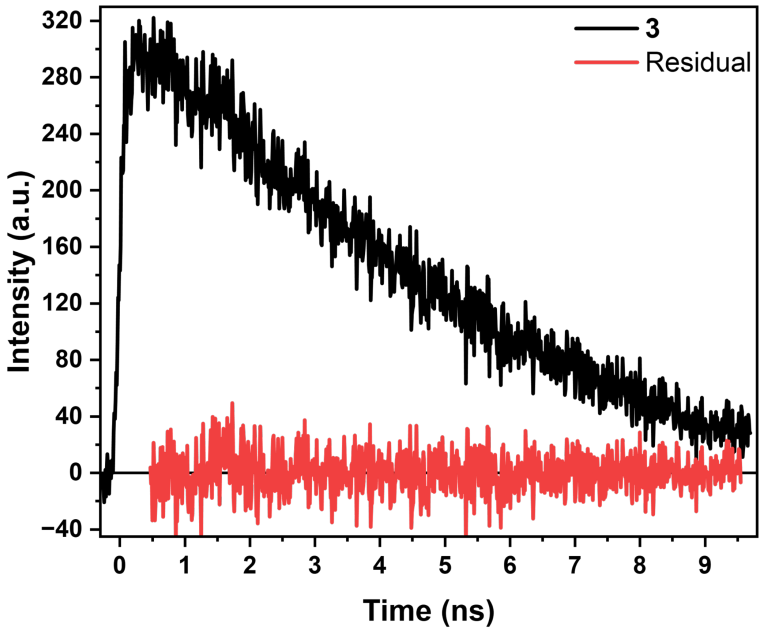

Figure S15. Kinetic emission decay of **3** collected in MeCN by excitation at 570 nm (0.2 nJ/pulse) on a LifeSpec II TCSPC. Single-wavelength kinetics analysis determined lifetime of τ_{PL} = 7.7 ± 0.3 ns

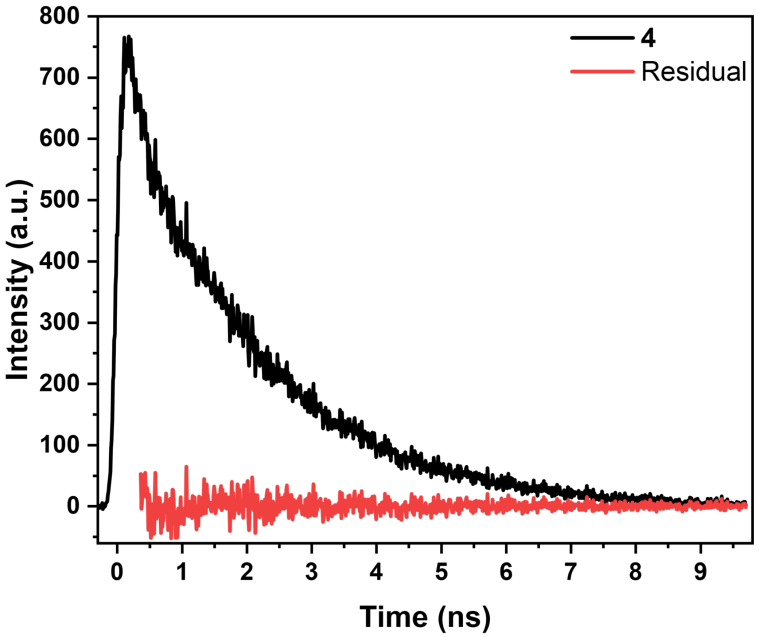

Figure S16. Kinetic emission decay of **4** collected in MeCN by excitation at 570 nm (0.2 nJ/pulse) on a LifeSpec II TCSPC. Single-wavelength kinetics analysis determined lifetime of τ_{PL} = 2.07 ± 0.01 ns

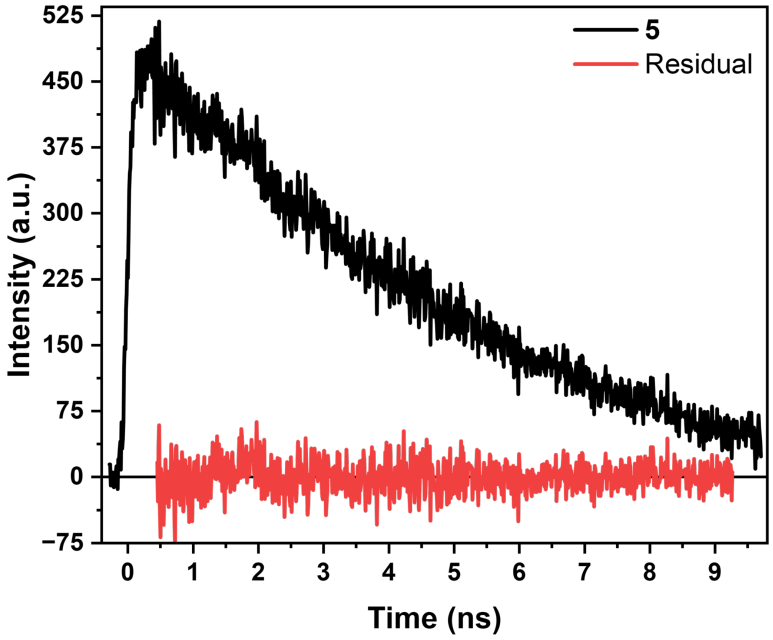

Figure S17. Kinetic emission decay of **5** collected in MeCN by excitation at 570 nm (0.2 nJ/pulse) on a LifeSpec II TCSPC. Single-wavelength kinetics analysis determined lifetime of τ_{PL} = 6.8 ± 0.2 ns

Transient Absorption Spectroscopy – Characterization of the Excited State Manifold:

Table S1. Determination of the S_1-T_1 Exchange Energy ($\Delta E_{S\text{-}T}$) of **1** in THF and MeCN.

	λ_{abs} (nm)	E_{1MMLCT} (cm^{-1})	λ_{PL} (77 K) (nm)[a]	E_{3MMLCT} (cm^{-1})	$S_1 - T_1$ Exchange Energy (cm^{-1})[b]
THF	547.6	18,262	653	15,314	2,949
MeCN	547.6	18,262	643.5	15,540	2,721

[a]77K measurements collected in 2-MeTHF and butyronitrile, respectively; [b]calculated based on peak maximum

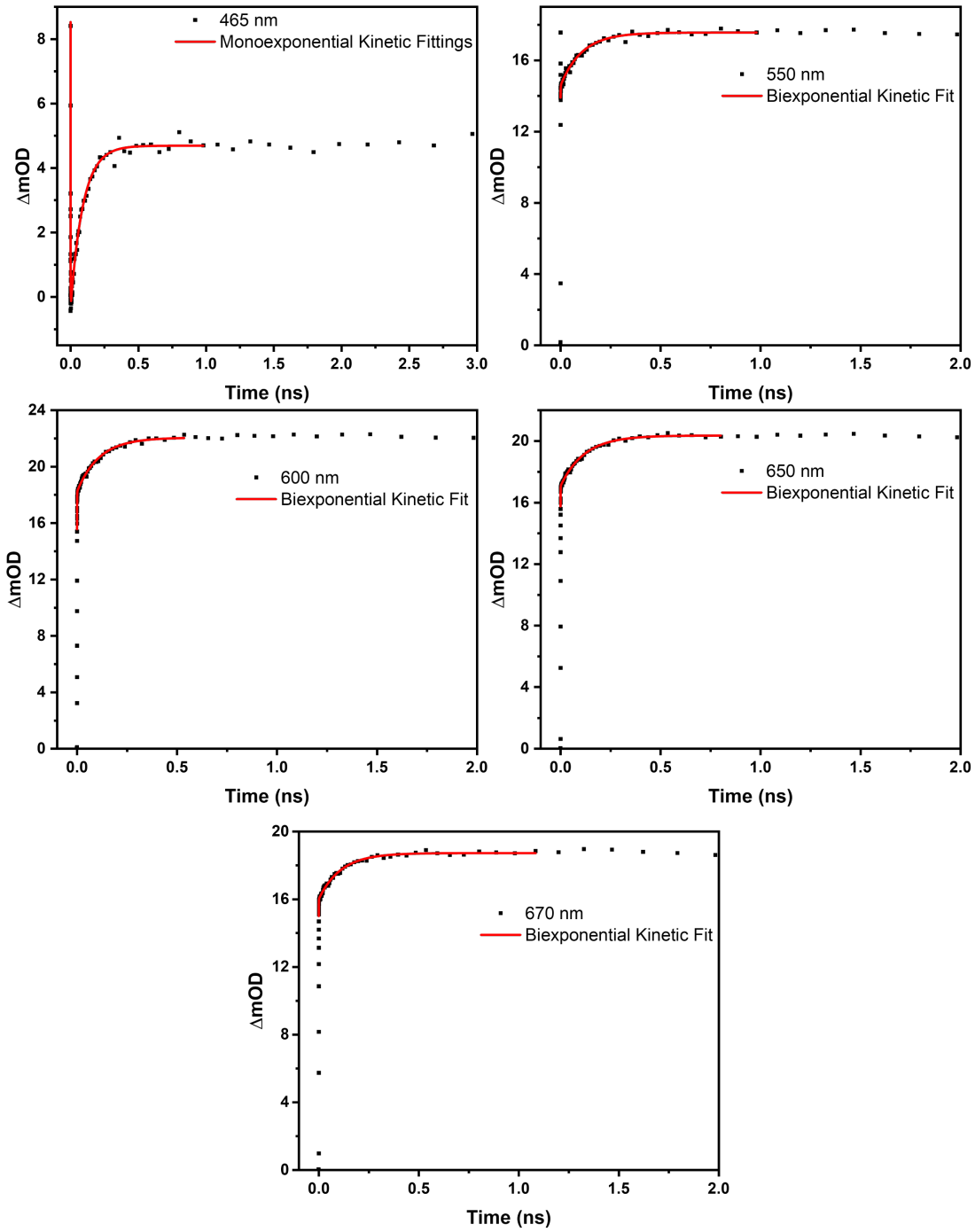

Figure S18. Single-wavelength kinetic decays and biexponential fits of **1**, collected in MeCN following 500 nm (1.5 μJ/pulse) excitation, monitored at **a)** 465 nm (τ_1 = 0.5 ± 0.1 ps; τ_2 = 92 ± 3 ps), **b)** 550 nm (τ_1 = 0.9 ± 0.3 ps; τ_2 = 107 ± 6 ps), **c)** 600 nm (τ_1 = 0.45 ± 0.03 ps; τ_2 = 110 ± 4 ps), and **d)** 650 nm (τ_1 = 0.42 ± 0.05 ps; τ_2 = 119 ± 4 ps), **e)** 670 nm (τ_1 = 0.41 ± 0.07 ps; τ_2 = 110 ± 5 ps)

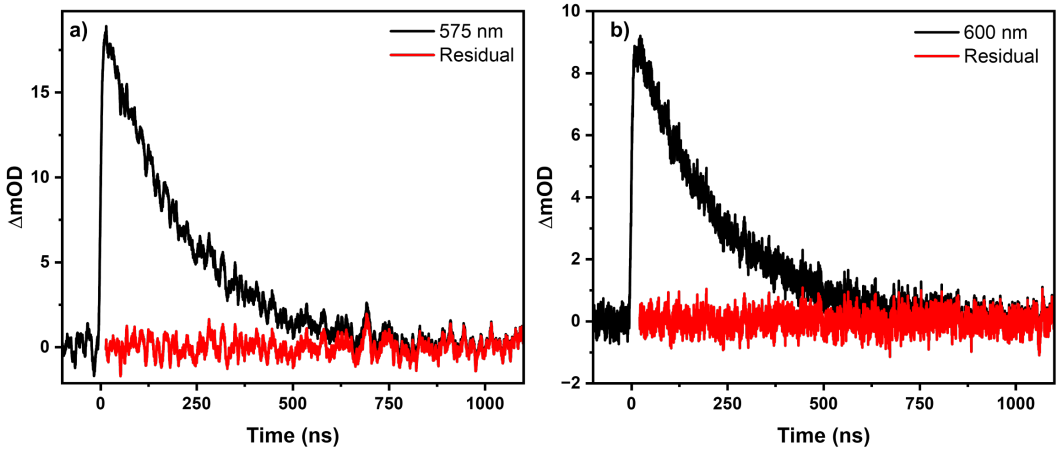

Figure S19. Nanosecond transient absorption single wavelength kinetics of **1** for the determination of the ^{3}MMLCT excited state lifetime (τ_3) in MeCN (500 nm, 1.2 mJ.pulse). **a)** 575 nm (τ_3 = 208.1 ± 0.7 ns) and **b)** 600 nm (τ_3 = 216 ± 1 ns).

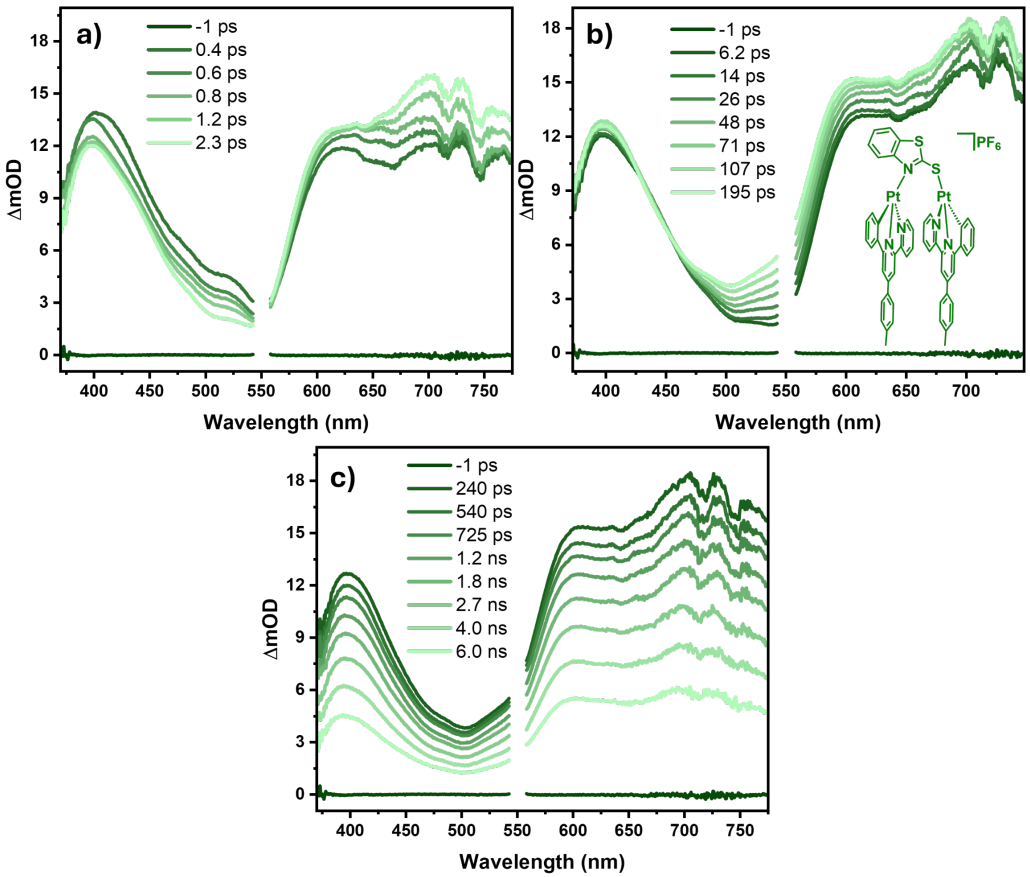

Figure S20. Femtosecond transient absorption difference spectra of **2**, collected in MeCN following 550 nm (1.2 µJ/pulse). **a)** first 2 ps, τ_1; **b)** 6 ps to 195 ps, τ_2 ; **c)** 240 ps to 6 ns, τ_3.

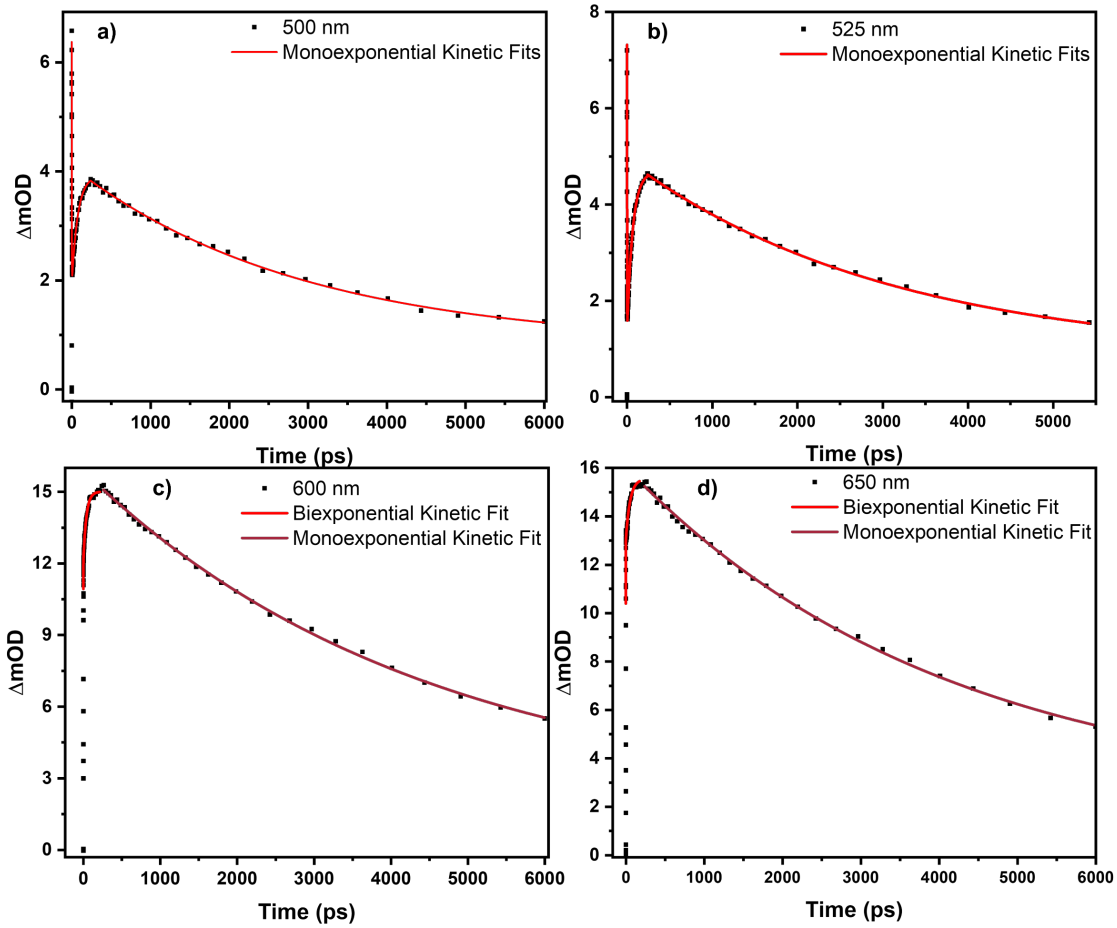

Figure S21. Femtosecond single-wavelength kinetic decays and biexponential fits of **2**, collected in MeCN following 550 nm (1.2 μJ/pulse) excitation, monitored at **a)** 500 nm **(**τ_1 = 1.22 ± 0.07 ps; τ_2 = 71 ± 3 ps; τ_3 = 3.0 ± 0.1 ns), **b)** 525 nm (τ_1 = 1.2 ± 0.3 ps; τ_2 = 66 ± 1 ps; τ_3 = 3.1 ± 0.1 ns), **c)** 600 nm (τ_1 = 0.77 ± 0.9 ps; τ_2 = 43 ± 1 ps; τ_3 = 4.4 ± 0.2 ns), and **d)** 650 nm (τ_2 = 54 ± 7 ps; τ_3 = 4.3 ± 0.2 ns).

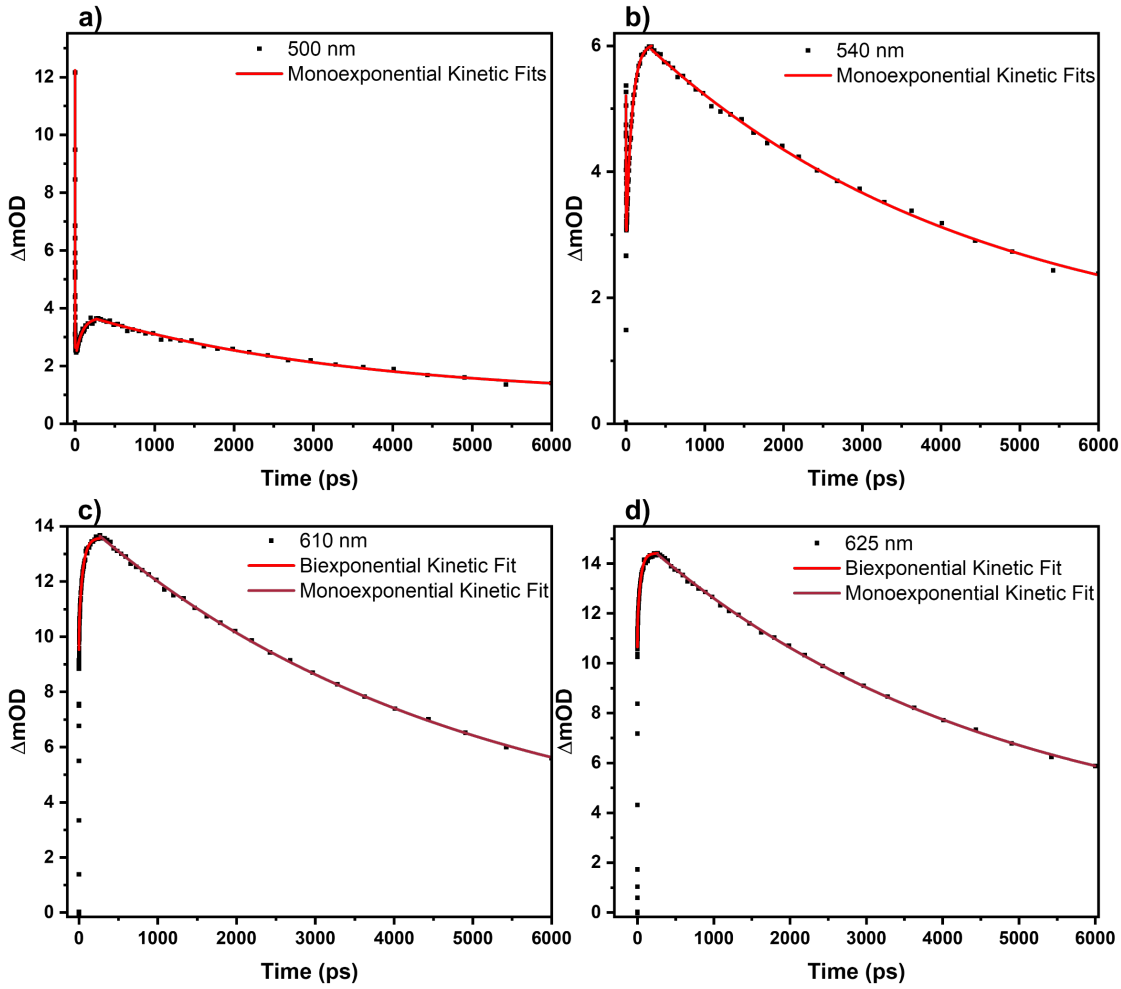

Figure S22. Femtosecond single-wavelength kinetic decays and biexponential fits of **3**, collected in MeCN following 550 nm (1.2 μJ/pulse) excitation, monitored at **a)** 500 nm (τ_1 = 0.83 ± 0.03 ps; τ_2 = 84 ± 9 ps; τ_3 = 3.5 ± 0.3 ns), **b)** 540 nm (τ_1 = 1.4 ± 0.2 ps; τ_2 = 74 ± 1 ps; τ_3 = 4.2 ± 0.2 ns), **c)** 610 nm (τ_2 = 50 ± 1 ps; τ_3 = 4.7 ± 0.1 ns), and **d)** 625 nm (τ_1 = 2.2 ± 0.2 ps; τ_2 = 42 ± 1 ps; τ_3 = 4.6 ± 0.1 ns).

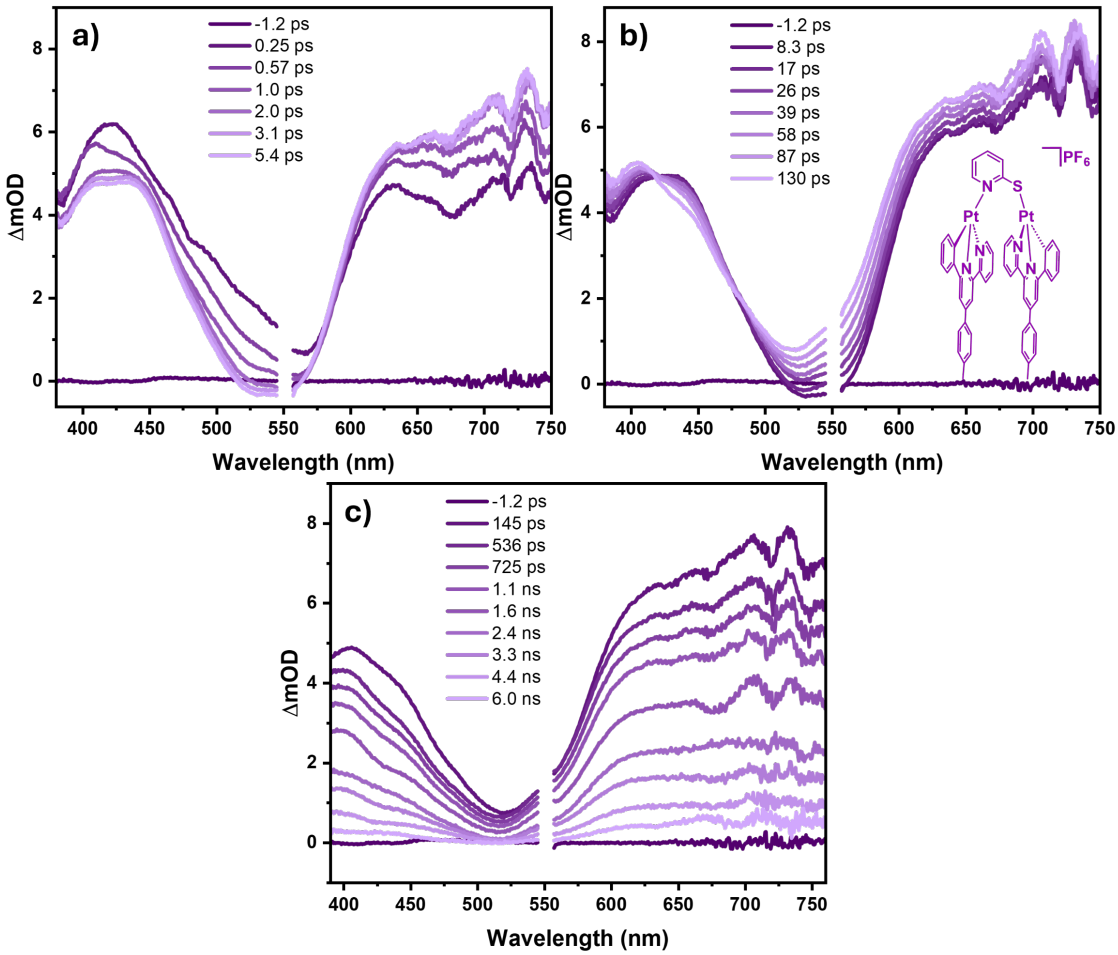

Figure S23. Femtosecond transient absorption difference spectra of **4**, collected in MeCN following 550 nm (1.2 μJ/pulse). **a)** first 5 ps, τ_1; **b)** 8 ps to 130 ps, τ_2 ; **c)** 145 ps to 6 ns, τ_3.

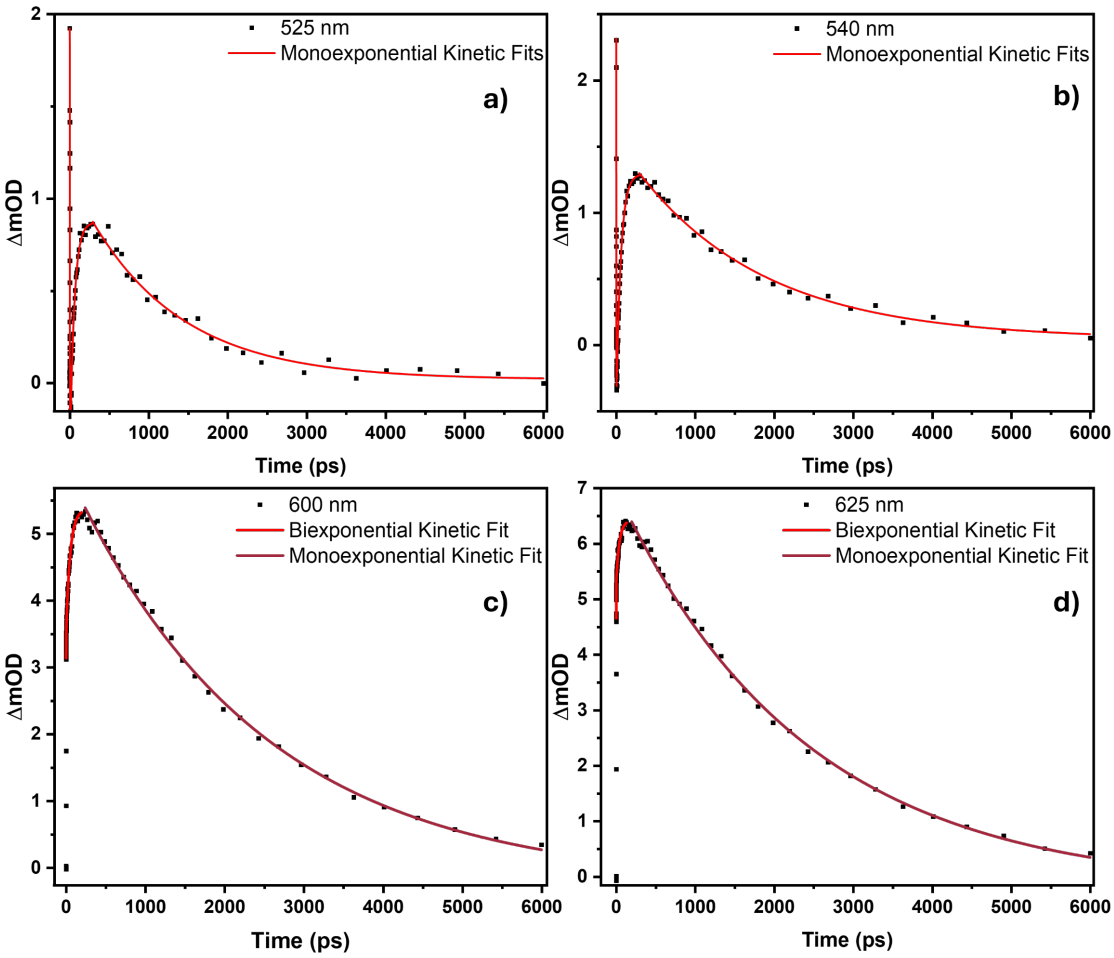

Figure S24. Femtosecond single-wavelength kinetic decays and biexponential fits of **4**, collected in MeCN following 550 nm (1.2 μJ/pulse) excitation, monitored at **a)** 525 nm (τ_1 = 1.0 ± 0.1 ps; τ_2 = 55 ± 2 ps; τ_3 = 1.17 ± 0.08 ns), **b)** 540 nm (τ_1 = 1.1 ± 0.2 ps; τ_2 = 57 ± 1 ps; τ_3 = 1.63 ± 0.08 ns), **c)** 600 nm (τ_2 = 51 ± 3 ps; τ_3 = 2.40 ± 0.09 ns), and **d)** 625 nm (τ_2 = 40 ± 6 ps; τ_3 = 2.37 ± 0.08 ns).

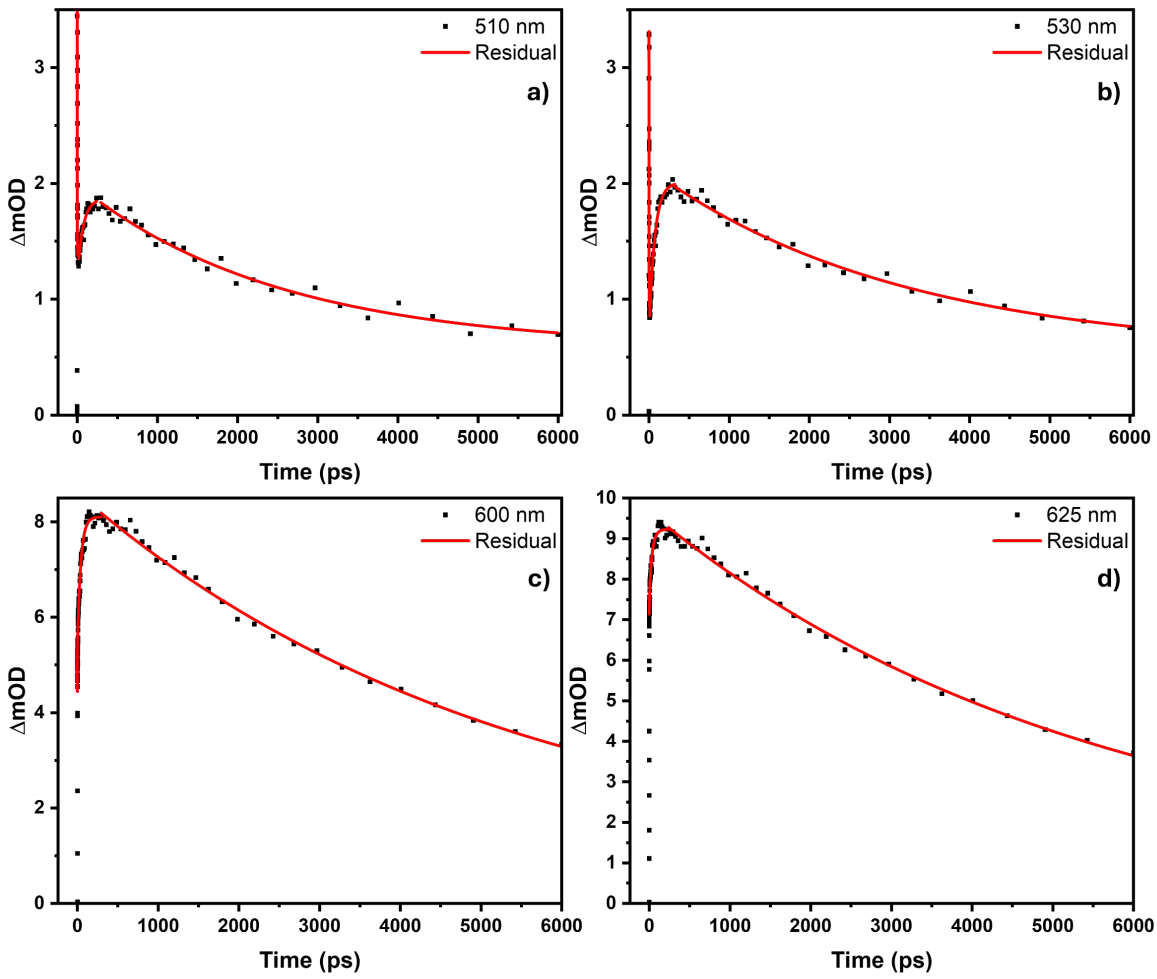

Figure S25. Femtosecond single-wavelength kinetic decays and biexponential fits of **5**, collected in MeCN following 550 nm (1.2 μJ/pulse) excitation, monitored at **a)** 510 nm (τ_1 = 1.22 ± 0.08 ps; τ_2 = 58 ± 5 ps; τ_3 = 2.6 ± 0.5 ns), **b)** 530 nm (τ_1 = 0.97 ± 0.04 ps; τ_2 = 64 ± 2 ps; τ_3 = 3.1 ± 0.4 ns), **c)** 600 nm (τ_1 = 1.1 ± 0.3 ps; τ_2 = 41 ± 3 ps; τ_3 = 5.3 ± 0.6 ns), and **d)** 625 nm (τ_2 = 36 ± 4 ps; τ_3 = 5.4 ± 0.6 ns).

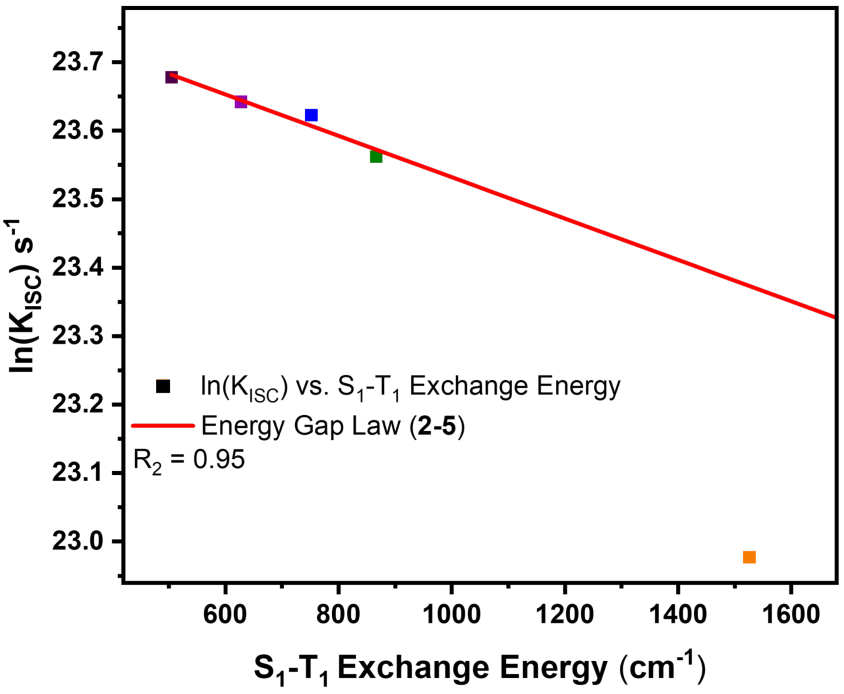

Figure S26. Energy gap law linear fitting describing the relationship between the rate of (proposed) intersystem crossing rate with the S_1-T_1 Exchange energy in cm^{-1}. The linear relationship was established only for the points corresponding to **2-5** (top left), and the orange point corresponding to complex **1** is provided as a comparison.